

Theory for spin and orbital orderings in high temperature phases in YVO_3

Theja. N. De Silva^{a,b}, Anuvrat Joshi^c, Michael Ma^{a,d}, and Fu Chun Zhang^{a,e}

^aDepartment of Physics, University of Cincinnati, Cincinnati Ohio 45221

^bDepartment of physics, University of Ruhuna, Matara, Sri Lanka

^c National High Magnetic Field Laboratory, Florida State University, Tallahassee, FL 32310

^d Department of Physics, Chinese University of Hong Kong, Shatin, Hong Kong

^e Institute of Theoretical Physics, Chinese Academy of Sciences, Beijing, China

Motivated by the recent neutron diffraction experiment on YVO_3 , we consider a microscopic model where each V^{3+} ion is occupied by two $3d$ electrons of parallel spins with two fold degenerate orbital configurations. The mean field classical solutions of the spin-orbital superexchange model predicts an antiferro-orbital ordering at a higher temperature followed by a C-type antiferromagnetic spin ordering at a lower temperature. Our results are qualitatively consistent with the observed orbital phase transition at ~ 200 K and the spin phase transition at ~ 114 K in YVO_3 .

I. INTRODUCTION

The transition metal perovskite oxides exhibit many interesting physical phenomena. In some of these compounds, the orbital degrees of freedom play an important role in their magnetic properties due to the strong spin-orbital coupling [1, 2, 3]. Examples include the Mott-Hubbard type insulators YVO_3 and $LaVO_3$, which show very unusual magnetic properties. Although the early experiments on YVO_3 and $LaVO_3$ were reported back in the mid 1970's [4, 5, 6], there has been renewed interest in the past decade on these materials [7, 8, 9, 10, 11, 12, 13, 14, 15]. There are two magnetic phases in YVO_3 : C-type antiferromagnetic order (ferromagnetic chains along the z-axis which stagger within the x-y plane) at temperature $114\text{K} > T > 77\text{K}$, and G-type antiferromagnetic order (staggered in all three directions) at temperature $T < 77\text{K}$ [4, 5, 6, 7]. The magnetic order in $LaVO_3$ is always C-type. The microscopic mechanism leading to the difference between these two compounds is still under investigation, and it might be related to the fact that the crystal structure at room temperature is distorted in YVO_3 but almost undistorted in $LaVO_3$. It is generally believed that the relevant orbital degrees of freedom, the degenerate or almost degenerate $3d - t_{2g}$ states are crucial to the observed magnetic properties.

There have also been interesting theoretical studies related to these magnetic behaviors [16, 17, 18, 19, 20, 21, 22, 23]. In particular, Khaliullin *et.al* [19] considered a spin-orbital Hamiltonian starting with 3-fold degenerate t_{2g} orbitals, and compared the free energies between the C-type and G-type spin states in YVO_3 by including an explicit Jahn-Teller energy in the model.

Very recently, Blake *et.al* [15] reported neutron diffraction experiment in YVO_3 , which shows clear evidence that the orbital ordering has a sudden change from high temperature G-type to low temperature C-type at the 77K magnetic phase transition, manifested by a change in the Jahn-Teller type of distortion. The data also show clear evidence for the orbital transition from high temperature disordered phase to the G-type ordered phase at

~ 200 K. This has motivated us to study the spin-orbital ordering in YVO_3 .

In this paper, we consider a microscopic model for insulating YVO_3 , where each V-ion has two electrons with parallel spins favored by the large Coulomb repulsion and the Hund's coupling. Among the three t_{2g} orbitals, the d_{xy} orbital is favored by the crystal field and always singly occupied, while the other electron occupies either d_{xz} or d_{yz} states. This description is consistent with the neutron diffraction experiment [15]. We consider the superexchange interaction of the model and derive an effective Hamiltonian for YVO_3 . We then study the mean field classical solutions of the model, and examine the spin and orbital orderings. We find a G-type orbital ordering at a higher temperature followed by an additional C-type spin ordering at a lower temperature. Our result is consistent with the observed orbital phase transition at ~ 200 K, and spin phase transition at 114K in YVO_3 . In this scenario, the orbital ordering at ~ 200 K is of the electronic origin, and the lattice distortion at ~ 200 K observed in the experiment is a consequence of the orbital ordering and the electron-lattice coupling. The superexchange interaction alone considered in our model does not explain the phase transition at 77K, which may require other interactions such as the Jahn-Teller effect as proposed in previous articles [17, 19].

This paper is organized as follows. In Section II, we examine a multi-band Hubbard model at electron density 2 electron per site, and consider the limit of large Coulomb repulsion and the large Hund's coupling. We then derive an effective Hamiltonian based on the superexchange mechanism. In Section III, we discuss the mean field classical solutions of the model, and examine the phase diagram for the orbital and spin orderings. A brief summary is given in Section IV.

II. MODEL

In YVO_3 , the vanadium electron configuration is $3d^2$. The compound has a cubic crystal structure, and each

V ion is surrounded by six oxygen ions. Due to the cubic crystal field, the five-fold degenerate $3d$ orbitals are split into a higher energy doublet of e_g orbitals and a lower energy triplet t_{2g} orbitals. At low temperatures and for low energy physics, the relevant orbitals are the three-fold t_{2g} orbitals: d_{xy} , d_{yz} , d_{zx} . In the strong coupling limit, the on-site Coulomb repulsion between the two electrons in the $3d$ states and the Hund's coupling are much larger than the intersite electron hopping amplitudes, the system is a Mott insulator with each V -ion having two localized electrons of parallel spins in two out of three degenerate t_{2g} orbitals. This scenario appears to be consistent with experiments.

As indicated in the recent diffraction experiment [15], the cubic crystal is distorted at room temperature. As a result, the V -O bond distances are anisotropic. Here we consider the structure at room temperature, where the V -O bond distance along c -axis (perpendicular axis) is the smallest (see figure 1). This crystal structure further splits the t_{2g} states. The d_{xy} orbital has a lower energy, and becomes always singly occupied. The other d-electron is either in d_{yz} or d_{zx} orbital. In the diffraction experiment [15], the data also indicate a smaller difference in V -O bond lengths in the xy plane, which we shall neglect here for simplicity.

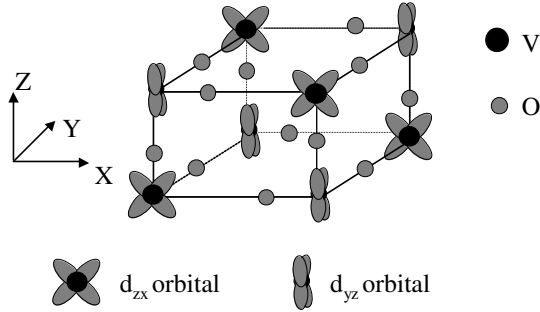


FIG. 1: Idealized crystal structure for YVO_3 studied in this paper. $V - O$ bond distance along the z -direction is shorter. The shown orbital represent configurations $d_{xy}d_{yz}$ or $d_{xy}d_{zx}$.

The atomic Hamiltonian [21] is then given by $H_0 = \sum_i H_i$, where the sum over i runs all the V-sites, and

$$H_i = \frac{1}{2} \sum_{mm',\sigma\sigma'} (1 - \delta_{mm'}\delta_{\sigma\sigma'}) U_{mm'} n_{im\sigma} n_{im'\sigma'} - J \sum_{mm',\sigma} \left(n_{im\sigma} n_{im'\sigma} + c_{im\sigma}^\dagger c_{im-\sigma} c_{im'-\sigma}^\dagger c_{im'\sigma} \right. \\ \left. - c_{im'-\sigma}^\dagger c_{im'\sigma}^\dagger c_{im\sigma} c_{im-\sigma} \right) + \sum_{m,\sigma} \Delta_m n_{m\sigma}. \quad (1)$$

In the above Hamiltonian, $c_{im\sigma}^\dagger$ ($c_{im\sigma}$) creates (annihilates)

an electron of orbital m and spin σ at site i , $n_{im\sigma} = c_{im\sigma}^\dagger c_{im\sigma}$. $\Delta_1 = \Delta_2 = 0$, and $\Delta_3 = \Delta < 0$, with $m = 1, 2, 3$ representing orbitals d_{yz} , d_{zx} , d_{xy} respectively. $U_{mm'}$ is the on-site direct interaction, and J is the exchange interaction, or the Hund's coupling. For the t_{2g} orbitals, $U_{mm} = U = U_{mm'} + 2J$ for $m' \neq m$. In the case $U, J > \Delta$, this Hamiltonian leads to an atomic ground state with each $V - 3d^2$ ion having a total spin $S = 1$ with two-fold degenerate orbital configurations (d_{xy}, d_{xz}) and (d_{xy}, d_{yz}).

We next introduce the intersite hopping Hamiltonian H_t , given by

$$H_t = \sum_{\langle ij \rangle} \sum_{mm',\sigma} \left(t_{m,m'}^{ij} c_{i,m,\sigma}^\dagger c_{j,m',\sigma} + h.c. \right) \quad (2)$$

where the sum runs over all the nearest neighbor V-V pairs, and $t_{m,m'}^{ij}$ is the electron hopping integral between two sites i and j from orbital m to orbital m' . Since the most important contribution to the hopping integrals is from the path via the $2p$ state of the O-ion between the two neighboring V-ions, the hopping integrals are diagonal in the present problem due to the cubic symmetry. Namely, we have $t_{m,m'}^{ij} = t_m^{ij} \delta_{m,m'}$. Therefore, there are only two independent hopping parameters, $t_{11}^z = t_{22}^z = t_{\perp}$, and $t_{22}^x = t_{33}^x = t_{11}^y = t_{33}^y = t_{\parallel}$, with the super-index indicating the direction of the two sites. In the limit $t_{\perp}, t_{\parallel} \ll U, J, \Delta$, the system is an insulator with spin 1 on each V-ion. However, the virtual hopping introduces an effective intersite coupling of spins and the occupied orbitals. The effective Hamiltonian for $H = H_0 + H_t$ can be derived by applying perturbation theory to second order in t_{\perp} or t_{\parallel} .

Let $|\phi_{ij}\rangle = |s_i^z, \tau_i^z, s_j^z, \tau_j^z\rangle$ be a ground state of H_0 for two V-ions i, j , where $s^z = 1, 0, -1$ is the spin z -component, and τ is a pseudospin-1/2 operator for the orbitals: $\tau^z = 1/2$ if d_{yz} is occupied, and $\tau^z = -1/2$ if d_{xz} is occupied. The matrix element of the ground states of the two V-ions can be calculated within the second order perturbation theory, and it is given by,

$$\langle \phi_{kl} | H_{eff} | \phi_{ij} \rangle = \sum_I \frac{\langle \phi_{kl} | H_t | I \rangle \langle I | H_t | \phi_{ij} \rangle}{E_0 - E_I} \quad (3)$$

where the sum is over all the intermediate eigenstates $|I\rangle$ of H_0 corresponding to the eigen energy E_I , and E_0 is the ground state energy of H_0 . The electronic configuration of the intermediate state $|I\rangle$ is $3d^3$ on one V-ion and $3d^1$ on the other. In the Appendix, we list all the states for $V - 3d^3$, and the corresponding energy difference $E_I - E_0$. The effective Hamiltonian can be derived from these matrix elements, and it is given, in terms of spin-1 operator \mathbf{S} and pseudospin-1/2 operator τ , as below,

$$H_{eff} = \sum_{\langle ij \rangle, \nu} \sum_{\sigma=\pm 1} K_{\sigma}^{\nu} (\tau_i, \tau_j) (\mathbf{S}_i \cdot \mathbf{S}_j + \sigma), \quad (4)$$

where $\nu = x, y, z$, and $2K_+^\nu$ and $2K_-^\nu$ are the intersite orbital couplings for parallel and antiparallel spins respectively. We choose the energy unit to be t_{\parallel}^2/U , and denote $\eta = J/U$, $\eta_{\frac{3}{2}} = 1/(1-3\eta)$, $\eta_{\frac{1}{2}} = 1/(1+2\eta)$, and $Q = t_{\perp}/t_{\parallel}$. K_{\pm}^ν can be expressed in terms of parameters Q and η , and are given below.

$$\begin{aligned}
K_+^{(x,y)} &= \eta_{\frac{3}{2}}(\tau_{iz}\tau_{jz} - \frac{1}{4}), \\
K_+^z &= 2Q^2\eta_{\frac{3}{2}}(\vec{\tau}_i \cdot \vec{\tau}_j - \frac{1}{4}), \\
K_-^{(x,y)} &= \alpha(\tau_{iz}\tau_{jz} - \frac{1}{4}) + \frac{3}{4}(1 + \eta_{\frac{1}{2}}) \\
&\quad + \frac{(-1)^{n_{x,y}}}{4}(1 + \eta_{\frac{1}{2}})(\tau_{iz} + \tau_{jz}), \\
K_-^z &= Q^2\{2\alpha(\tau_{iz}\tau_{jz} - \frac{1}{4}) + \frac{1}{2}(1 + \eta_{\frac{1}{2}}) \\
&\quad - \frac{1}{3}(\eta_{\frac{3}{2}} - 1)(\tau_i^+\tau_j^- + \tau_i^-\tau_j^+) \\
&\quad - \frac{1}{2}(1 - \eta_{\frac{1}{2}})(\tau_i^+\tau_j^+ + \tau_i^-\tau_j^-)\}. \quad (5)
\end{aligned}$$

In the above equations, $\alpha = -\frac{1}{6}(1 + 2\eta_{\frac{3}{2}} - 3\eta_{\frac{1}{2}})$, and $(-1)^{n_x} = -1$, $(-1)^{n_y} = 1$.

We first discuss the intersite pseudospin couplings between two parallel spins. In this case, the pseudospin has a $SU(2)$ symmetry along z -direction. Along x - or y -direction, however, the virtual hopping integral for orbital 2 or orbital 1 vanishes, so there is no exchange term in the pseudospin, and $K_+^{(x,y)}$ is of the Ising form. The pseudospin coupling between the two V-ions of antiparallel spins is quite different. There is a linear term $(\tau_{iz} + \tau_{jz})$ along x - or y -direction, which either favors d_{zx} or d_{yz} orbital occupation to gain energy via the virtual hopping process. The pseudospin coupling along z -direction includes both the exchange term $(\tau_i^+\tau_j^- + h.c.)$ and the pair flip term $(\tau_i^+\tau_j^+ + h.c.)$. In spite of an isotropic matrix in the z -direction, the orbital Hamiltonian is not $SU(2)$ symmetric because of the presence of Hund's coupling. In particular, the pair flip term is related to superexchange processes involving those intermediate states listed in Table II that are split in energy due to Hund's coupling. To illustrate this point further, we consider a pair of V-ions along z -direction with antiparallel spins and pseudospins are $\tau_{iz} = \tau_{jz} = 1/2$. The relevant intermediate states in the superexchange are the states listed in the second and the fifth rows in Table II. Because these states have different energies, there is non-zero amplitude for the pseudospins to flip to $\tau_{iz} = \tau_{jz} = -1/2$. The pseudospin pair flip process is actually quite common in orbital physics. For example, there are pair flip terms in the effective Hamiltonian for spin-1/2 systems with orbital degeneracy derived by Castellani et al. [21].

In the limit $J/U = 0$, $\eta_{\frac{3}{2}} = \eta_{\frac{1}{2}} = 1$, and $\alpha = 0$. We have $K_-^z = Q^2$, and $K_-^{(x,y)} = -\frac{(-1)^{n_{x,y}}}{2}(\tau_{iz} + \tau_{jz}) + \frac{3}{2}$. The orbital coupling between the two V-ions of antipar-

allel spins vanishes, and the orbital coupling between the two V-ions of parallel spins remains to be pseudospin $SU(2)$ symmetric along z -direction and pseudospin Ising symmetric along x - or y -directions. For $J/U = 0$, the lack of the global pseudospin $SU(2)$ symmetry is due to the anisotropic hopping integrals in the system.

Our effective Hamiltonian here is different from the Hamiltonian proposed previously by Khaliullin et al. [19]. These authors considered a model with 3-fold t_{2g} orbital degeneracy, while we consider a 2-fold orbital degeneracy with d_{xy} orbital being always singly occupied. Below we shall compare the two Hamiltonians by considering the spin-orbital coupling between two V-ions along z -direction, namely H_{ij} , with $j = i + z$. This may be carried out by imposing the orbital d_{xy} being always singly occupied in the Hamiltonian of Khaliullin et al. We find that the $\tau_{iz}\tau_{jz}$ terms are the same in the two theories. However, the Hamiltonian of Khaliullin et al. does not include the pseudospin flip term $(\tau_i^+\tau_j^+ + h.c.)$. As we illustrated above, the pseudospin flip term is non-zero. As we shall see in the next section, this pair flip term does not affect the mean field results, which depend only on the z -components of pseudospins in the present case. It will be an interesting question to examine if the pseudospin flip term is important to the orbital fluctuations.

III. MEAN FIELD THEORY AND THE PHASE DIAGRAM

We start with the classical solutions of H_{eff} . The Hamiltonian has a global $SU(2)$ symmetry in spin space, so that we can assume the spin ordering along the z -direction. The Hamiltonian is invariant under the simultaneous transformation of global $Z(2)$ (reversing orbitals at all sites) and a 90° rotation of the lattice about the z -axis. In general, we should consider orbital ordering along an arbitrary orientation. However, for the present problem, the orbital z -component terms are always larger or equal to the x - or y -component terms in K_{\pm}^ν of Eq. (5). Therefore, we can discuss the classical solutions by considering the z -component of the orbital ordering only [24]. In other words, the classical solutions are the same as the Ising solutions in the present case. In Table I, we show the energies per site in various classical states. Note that $\eta_{\frac{1}{2}} \leq 1$, and $\eta_{\frac{3}{2}} \geq 1$, where the equality holds if and only if $J = 0$. We consider below the case with non-zero Hund's coupling $J > 0$. In this case, the two states listed in Table I with C-type antiferro-orbital (CO) configuration have higher energies. Also, we can see that the G-type antiferromagnetic spin (GS) and G-type antiferro-orbital (GO) phase has a higher energy than the CS-GO phase. Therefore, the ground state is either ferromagnetic spin (FS) and GO, or CS-GO. In both FS-GO and CS-GO phases, the orbital is antiparallel in all three directions, favored by the combination of the symmetries

in hopping integrals (due to the cubic crystal symmetry) and the Hund's coupling. The asymmetry between the spin configuration along the z-axis and in the x-y plane is a result of the splitting of the d_{xy} orbital level from the other two t_{2g} orbitals. As expected, the FS-GO phase is energetically more favored at a larger J where the Hund's coupling dominates, and the CS-GO phase is more favored at a smaller J . It may be helpful to understand these two possible ground states by examining the following limiting cases more explicitly. In the limit of large Hund's coupling, $\eta \rightarrow 1/3$, the terms in the energy expression in Table I proportional to $\eta_{\frac{3}{2}}$ dominate. Hence the FS-GO phase has the lowest energy. In the limit $J \rightarrow 0^+$, $\eta_{\frac{1}{2}} \rightarrow 1 - 0^+$, and $\eta_{\frac{3}{2}} \rightarrow 1 + 0^+$, so that the CS-GO phase has the lowest energy.

We now discuss the finite temperature phases and their transitions. We introduce three types of order parameters, namely the spin order parameter $m_i = \langle S_{iz} \rangle$, the orbital order parameter $r_i = \langle \tau_{iz} \rangle$, and the spin-orbital order parameter $q_i = \langle S_{iz} \tau_{iz} \rangle$. We shall consider the order parameters corresponding to the FS-GO and CS-GO phases, since other ordered states are not energetically favorable. In both the FS-GO and CS-GO phases, we divide the lattice into two sublattices A and B accordingly. For the FS-GO ordering, we consider $m_i = m$ for all the sites i , and $r_i = r$ and $q_i = q$ for i at sublattice A and $r_i = -r$ and $q_i = -q$ for i at sublattice B . For the CS-GO ordering, we consider $m_i = m$, $r_i = r$, and $q_i = q$ for i at sublattice A , and $m_i = -m$, $r_i = -r$, and $q_i = q$ for i at sublattice B . We use a mean field theory to examine the thermodynamically stable phases described by these order parameters, and neglect both quantum and thermal fluctuations. The effective Hamiltonian H_{eff} is then approximated by,

$$H_{\text{MF}} = \sum_i (aS_{iz} + b\tau_{iz} + cS_{iz}\tau_{iz} + d) \quad (6)$$

In the above equations, coefficient a , b , c , d are functions of η , Q , as well as of the mean fields m , r , and q . They are given by, with the subscript upper (-) and lower (+) signs corresponding to the CS-GO and FS-GO phases, respectively,

$$\begin{aligned} a &= A_{\mp}mr^2 + D_{\mp}m, \\ b &= A_{\mp}m^2r - B_{\mp}r, \\ c &= -A_{\mp}(2m^2r^2 + q), \\ 2d &= -C_{\mp}m^2r^2 + E_{\mp}m^2 + Br^2 - A_{\mp}q^2, \end{aligned} \quad (7)$$

where $B = B_-$, and

$$\begin{aligned} A_{\pm} &= 4(\eta_{\frac{3}{2}} + \alpha)(Q^2 \pm 1), \\ B_{\pm} &= 4(\eta_{\frac{3}{2}} - \alpha)(Q^2 \mp 1), \\ C_{\pm} &= 4(\eta_{\frac{3}{2}} + \alpha)(Q^2 \pm \frac{1}{2}), \end{aligned} \quad (8)$$

$$\begin{aligned} D_{\pm} &= (1 + \eta_{\frac{1}{2}})(Q^2 \pm 3) - (\eta_{\frac{3}{2}} + \alpha)(Q^2 \pm 1), \\ E_{\pm} &= -(1 + \eta_{\frac{1}{2}})(Q^2 \pm \frac{3}{2}) + (\eta_{\frac{3}{2}} + \alpha)(Q^2 \pm \frac{1}{2}). \end{aligned}$$

The mean field Hamiltonian can be solved easily to obtain the thermal averages of S_{iz} , τ_{iz} , and $S_{iz}\tau_{iz}$, from which we obtain the following self-consistent equations for the order parameters m , r and q , (with β the inverse temperature)

$$\begin{aligned} \langle S_{iz} \rangle &= m = -\frac{2 \sinh(\beta a)}{(1 + 2 \cosh(\beta a))} \\ \langle \tau_{iz} \rangle &= r = -\frac{1}{2} \tanh(\beta b/2) \\ \langle S_{iz}\tau_{iz} \rangle &= q = -\frac{\sinh(\beta c/2)}{(1 + 2 \cosh(\beta c/2))}. \end{aligned} \quad (9)$$

The free energy per site in the mean field theory is given by

$$f = -\frac{1}{\beta} \ln \left(4 \cosh(\beta b/2) [1 + 2 \cosh(\beta c/2)] \right. \\ \left. \times [1 + 2 \cosh(\beta a)] \right) + d. \quad (10)$$

We solve the self-consistent equations for different ordered states at various temperatures. The phases studied are (i). paramagnetic spin (PS) and para-orbital (PO) state (PS-PO) with $m = r = q = 0$; (ii). CS-PO state with C-type spin ordering $m \neq 0$ and $r = q = 0$; (iii). PS-GO state with $r \neq 0$ and $m = q = 0$; (iv). CS-GO state; and (v). FS-GO state. In the states (iv) and (v), $m, r, q \neq 0$. When more than one set of MF solutions exist at a given temperature, we compare their free energies to determine the thermodynamically stable phase diagram.

In Fig. 2 and Fig. 3, we plot the phase diagrams obtained from the mean field theory for $Q = 1.3$ and $Q = 0.5$, respectively. The phase diagram for $Q = 1$ is qualitatively the same as that for $Q = 1.3$. The ground state is found to be CS-GO for smaller J/U , and FS-GO for larger J/U , consistent with our previous discussions. In general, the spin and orbital ordering occur at different temperatures. This feature is in distinction from the model for V_2O_3 for which spin and orbital order at the same temperature [25, 26]. Within the mean field theory, the phase transition between CS-GO and FS-GO is first order, and all other transitions between the different phases in Figs. 2 and 3 are second order. (The lattice distortion associated with the orbital ordering, which is not included in our model, may change the nature of the phase transition.)

In passing, we note that the spin-orbital ordering described by the order parameter q is always zero unless both the spins and the orbitals are ordered in the present system. This result indicates that the spin-orbital ordering parameter q introduced in our mean field theory

TABLE I: Mean field classical ground state energies for various phases.

Phase	Energy per site
G-type spin and G-type orbital (GS-GO)	$-\frac{2}{3} \left(5 + 2Q^2 + (1 + Q^2)\eta_{\frac{3}{2}} + 3\eta_{\frac{1}{2}} \right)$
C-type spin and G-type orbital (CS-GO)	$-\frac{2}{3} \left(5 + (1 + Q^2)\eta_{\frac{3}{2}} + 3\eta_{\frac{1}{2}} \right)$
G-type spin and C-type orbital (GS-CO)	$-\frac{1}{3} \left(10 + 3Q^2 + 2\eta_{\frac{3}{2}} + 3(2 + Q^2)\eta_{\frac{1}{2}} \right)$
C-type spin and C-type orbital (CS-CO)	$-\frac{2}{3} \left(5 + \eta_{\frac{3}{2}} + 3\eta_{\frac{1}{2}} \right)$
Ferro spin and G-type orbital (FS-GO)	$-2(1 + Q^2)\eta_{\frac{3}{2}}$

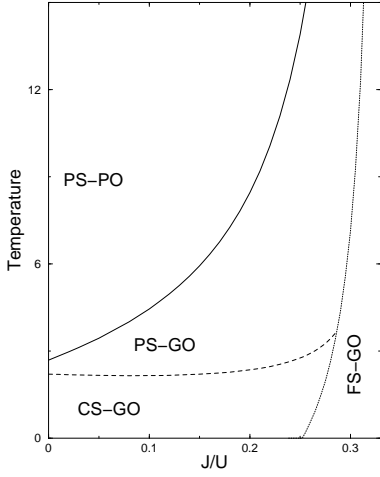


FIG. 2: Phase diagram for the anisotropic hopping parameter $Q = t_{\perp}/t_{\parallel} = 1.3$ in the parameter space of temperature and relative Hund's coupling J/U . Temperature is shown in units of t_{\parallel}^2/U . Solid line is the phase boundary between para-orbital (PO) and G-type antiferro-orbital (GO) states, the dashed line is the boundary between paramagnetic (PS) and C-type antiferromagnetic (CS) states, the dotted line is the phase boundary between PS and ferromagnetic (FS) states.

in addition to the spin order parameter m and the orbital order parameter r may not be as significant in the present problem in altering the qualitative physics as in the $SU(4)$ model [27].

In what follows, we shall focus on the phases relevant to YVO_3 , and discuss the sequential phase transitions from PS-PO to CS-GO. As we can see from Fig. 2, as the temperature decreases from the disordered state PO-PS, the system first undergoes a transition to the G-type antiferro-orbital ordered phase. Only at lower temperatures does the spin become C-type antiferromagnetic ordered. For smaller Q , the phase transitions depend on the Hund's coupling as we can see from Fig. 3. At intermediate J/U , the orbital transition temperature is higher than the spin's, while at smaller J/U , the spin

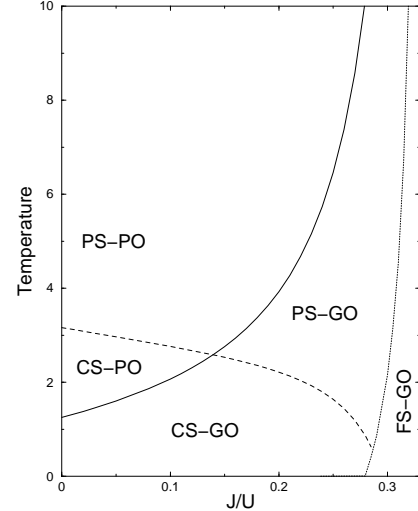


FIG. 3: Phase diagram for $Q = t_{\perp}/t_{\parallel} = 0.5$. For details, see Fig.2 caption.

transition temperature is higher than the orbital's. Since for YVO_3 , $Q \geq 1$, and the estimated values for U and J are $U \sim 4.5\text{eV}$ and $J \sim 0.68\text{eV}$ [17, 18], our theory suggests orbital ordering first at a higher temperature followed by a subsequent spin ordering at a lower temperature in YVO_3 . This is qualitatively consistent with the experimental findings for YVO_3 above 77K.

As recently reported by Blake *et.al* [15], the neutron diffraction experiment shows that the orbital ordering in YVO_3 takes place at $T_{GO} = 200\text{K}$, which is far above the antiferromagnetic ordering temperature $T_{CS} = 116\text{K}$. The orbital ordering is evidenced by the changes of the V-O bond lengths in the xy-plane. Our theory is consistent with these observations. Orbital ordering and lattice distortion are often observed simultaneously in experiments. It is usually difficult to distinguish if the lattice distortion is due to the orbital ordering or vice versa. Our theory suggests a scenario, in which the orbital ordering is of electronic origin, and the lattice distortion observed

above 77K is a consequence of the orbital ordering and the electron-phonon coupling.

In YVO_3 , as temperature decreases further, there is another phase transition at a lower temperature $T_{GS} = 77$ K, below which the system is in the G-type antiferromagnetic and C-type antiferro-orbital state. There have been proposals [17, 19] to attribute this lower temperature phase transition to the Jahn-Teller energy which favors C-type orbital ordering. It is an interesting issue to further understand the nature of the low temperature phase transition.

IV. SUMMARY

In summary, we have studied the electronic structure of the insulating YVO_3 , and derived an effective Hamiltonian based on the superexchange interaction. We started with the atomic limit where each $V - 3d^2$ has a spin-1 and two-fold degenerate orbital configurations ($d_{xy}d_{xz}$) and ($d_{xy}d_{yz}$). This consideration is consistent with the recent neutron diffraction experiment at $T > 77$ K. We studied the classical solutions of the model within mean field theory, and found G-type antiferro-orbital ordering at a higher temperature followed by a second phase transition where the spins become C-type ordered. Our theory explains the orbital and spin ordering of YVO_3 at temperatures $T > 77$ K. While our model does not explain the lower temperature phase of G-type spin ordering, which may require considerations in addition to the superexchange interaction, our theory provides a starting point for understanding the unusual magnetic properties of YVO_3 .

After we completed the present calculations, we learned of a very recent inelastic neutron scattering experiment of Ulrich et al. [28]. They reported an energy gap in the spin wave spectrum of YVO_3 in the C-type spin ordering phase, and they interpreted it as an evidence for the orbital Peierls state along the z-direction. The classical solutions we study here do not predict any spin or orbital Peierls transition. Quantum fluctuations or electron-lattice interactions may be responsible for this unusual state [20, 28].

This work was in part supported by DE/FG03-01ER45687, the URC Summer Student Fellowship at University of Cincinnati, and by the Chinese Academy of sciences. MM acknowledges the hospitality of the Hong Kong University of Science and Technology.

V. APPENDIX

In this Appendix, we present all the intermediate eigenstates $|I\rangle$ and their corresponding energy differences with the ground state, $E_I - E_0$, of the four t_{2g} electrons in two V-ions. These states are used in the second order

perturbation theory to derive the effective Hamiltonian H_{eff} in the text. The atomic ground states of the system are 6×6 -fold degenerate, with each ion occupied by two electrons of parallel spins in the orbital configurations ($d_{xy}d_{xz}$) or ($d_{xy}d_{yz}$). The atomic ground state energy is $E_0 = 2(U - 3J)$. The excited states $|I\rangle$ are $(V - 3d^1) - (V - 3d^3)$ with 6-fold degeneracy in $V - 3d^1$ ion. Here we consider the limiting case $U, J \gg \Delta$, and neglect the effect of Δ on the $V - 3d^3$ states. Within this approximation, these excited states are split into three multiples due to the Hund's coupling: 4×6 states with energy $(U - 3J + E_0)$, 10×6 states with energy $(U + E_0)$, and 6×6 states with energy $(U + 2J + E_0)$. The spin and orbital configurations of $V - 3d^3$ are listed in Table II.

- [1] N. F. Mott: Metal-Insulator Transitions (Taylor and Francis, London, 1990).
- [2] For a review, Y. Tokura and N. Nagaosa, Science, VOL 288, 462 (2000).
- [3] M. Imada, A. Fujimori and Y. Tokura, Rev. Mod. Phys. 70, 1039 (1998).
- [4] A. S. Borukhovich, G. V. Bazuv and G. P. Shveikin, Sov. Phys; Solid State 16, 191 (1974).
- [5] V. G. Zubkov, A. S. Borukhovich, G. V. Bazuv, I. I. Matveenko and G. P. Shveikin, Sov. Phys. JETP 39, 896 (1974).
- [6] V. G. Zubkov, G. V. Bazuv and G. P. Shveikin, Sov. Phys; Solid State 18, 1165 (1976).
- [7] H. Kawano, H. Yoshizawa and Y. Ueda, J. Phys. Soc. Jpn. 63, 2857 (1994).
- [8] H. C. Nguyen and J. B. Goodenough, Phys. Rev. B. 52, 324 (1995).
- [9] A. V. Mahajan et al., Phys. Rev. B 46, 10966 (1992).
- [10] J. Kikuchi, H. Yosuoka, Y. Kokubo and Y. Ueda, J. Phys. Soc. Jpn. 63, 3577 (1994).
- [11] F. Cintolesi, M. Corti, A. Rigamonti, G. Rossetti, P. Ghigna and A. Lascialfari, J. Appl. Phys. 79, 6624 (1996).
- [12] M. Corti, F. Cintolesi, A. Lascialfari and F. Rossetti, J. Appl. Phys. 81, 5286 (1997).
- [13] Y. Ren, T. T. M. Palstra, D. I. Khomskii, A. A. Nugroho, A. A. Menovsky and G. A. Sawatzky, Phys. Rev. B. 62, 6577 (2000).
- [14] S. Miyasaka, T. Okuda and Y. Tokura, Phys. Rev. Lett. 85, 5388 (2000).
- [15] G. R. Blake, T. T. M. Palstra, Y. Ren, A. A. Nugroho and A. A. Menovsky, Phys. Rev. Lett. 87, 245501 (2001).
- [16] T. Mizokawa and A. Fujimori, Phys. Rev. B 54, 5368 (1996).
- [17] T. Mizokawa, D. I. Khomskii and G. A. Sawatzky, Phys. Rev. B 60, 7309 (1999).
- [18] H. Sawada, N. Hamada, K. Terakura and T. Asada Phys. Rev. B 53, 12742 (1996).
- [19] G. Khaliullin, P. Horsch and A. M. Oles, Phys. Rev. Lett. 86, 3879 (2001).
- [20] S. Q. Shen, X. C. Xie and F. C. Zhang, Phys. Rev. Lett. 88, 027201 (2002).
- [21] C. Castellani, C. R. Natoli, and J. Ranninger, Phys. Rev.

TABLE II: Intermediate eigenstates $|I\rangle$ and corresponding energy differences $E_I - E_0$. The degeneracy shown is respected with the orbital configurations.

Eigenstate	Spin and orbital configuration	$E_I - E_0$
$(c_{1\uparrow}^\dagger c_{2\uparrow}^\dagger c_{3\uparrow}^\dagger) 0\rangle$		
$\frac{1}{\sqrt{3}}(c_{1\uparrow}^\dagger c_{2\downarrow}^\dagger c_{3\uparrow}^\dagger + c_{1\downarrow}^\dagger c_{2\uparrow}^\dagger c_{3\uparrow}^\dagger + c_{1\uparrow}^\dagger c_{2\uparrow}^\dagger c_{3\downarrow}^\dagger) 0\rangle$	$\frac{1}{\sqrt{3}}\left(\begin{array}{c} \uparrow\downarrow \\ \uparrow\uparrow \end{array}\right) + \left(\begin{array}{c} \downarrow\uparrow \\ \uparrow\uparrow \end{array}\right) + \left(\begin{array}{c} \uparrow\uparrow \\ \downarrow\downarrow \end{array}\right)$	$U - 3J$
$\frac{1}{\sqrt{3}}(c_{1\downarrow}^\dagger c_{2\uparrow}^\dagger c_{3\downarrow}^\dagger + c_{1\uparrow}^\dagger c_{2\downarrow}^\dagger c_{3\downarrow}^\dagger + c_{1\downarrow}^\dagger c_{2\downarrow}^\dagger c_{3\uparrow}^\dagger) 0\rangle$	$\frac{1}{\sqrt{3}}\left(\begin{array}{c} \downarrow\uparrow \\ \downarrow\uparrow \end{array}\right) + \left(\begin{array}{c} \uparrow\downarrow \\ \downarrow\downarrow \end{array}\right) + \left(\begin{array}{c} \uparrow\downarrow \\ \uparrow\downarrow \end{array}\right)$	
$(c_{1\downarrow}^\dagger c_{2\downarrow}^\dagger c_{3\downarrow}^\dagger) 0\rangle$		
$\frac{1}{\sqrt{2}}(c_{1\uparrow}^\dagger c_{1\downarrow}^\dagger c_{3\uparrow}^\dagger - c_{2\uparrow}^\dagger c_{2\downarrow}^\dagger c_{3\uparrow}^\dagger) 0\rangle$	$\frac{1}{\sqrt{2}}\left(\begin{array}{c} \uparrow\downarrow \\ \uparrow\uparrow \end{array}\right) - \left(\begin{array}{c} \downarrow\uparrow \\ \uparrow\uparrow \end{array}\right)$	U
$\frac{1}{\sqrt{2}}(c_{1\uparrow}^\dagger c_{1\downarrow}^\dagger c_{3\downarrow}^\dagger - c_{2\uparrow}^\dagger c_{2\downarrow}^\dagger c_{3\downarrow}^\dagger) 0\rangle$	$\frac{1}{\sqrt{2}}\left(\begin{array}{c} \uparrow\downarrow \\ \downarrow\downarrow \end{array}\right) - \left(\begin{array}{c} \downarrow\uparrow \\ \downarrow\downarrow \end{array}\right)$	(3-fold)
$\frac{1}{\sqrt{6}}(2c_{1\uparrow}^\dagger c_{2\uparrow}^\dagger c_{3\downarrow}^\dagger - c_{1\uparrow}^\dagger c_{2\downarrow}^\dagger c_{3\uparrow}^\dagger - c_{1\downarrow}^\dagger c_{2\uparrow}^\dagger c_{3\uparrow}^\dagger) 0\rangle$	$\frac{1}{\sqrt{6}}\left(2\begin{array}{c} \uparrow\uparrow \\ \downarrow\downarrow \end{array} - \begin{array}{c} \uparrow\downarrow \\ \uparrow\uparrow \end{array} - \begin{array}{c} \downarrow\uparrow \\ \uparrow\uparrow \end{array}\right)$	U
$\frac{1}{\sqrt{6}}(2c_{1\downarrow}^\dagger c_{2\downarrow}^\dagger c_{3\uparrow}^\dagger - c_{1\downarrow}^\dagger c_{2\uparrow}^\dagger c_{3\uparrow}^\dagger - c_{1\uparrow}^\dagger c_{2\downarrow}^\dagger c_{3\downarrow}^\dagger) 0\rangle$	$\frac{1}{\sqrt{6}}\left(2\begin{array}{c} \downarrow\downarrow \\ \uparrow\uparrow \end{array} - \begin{array}{c} \downarrow\uparrow \\ \downarrow\uparrow \end{array} - \begin{array}{c} \uparrow\downarrow \\ \downarrow\downarrow \end{array}\right)$	
$\frac{1}{\sqrt{2}}(c_{1\uparrow}^\dagger c_{2\downarrow}^\dagger c_{3\uparrow}^\dagger - c_{1\downarrow}^\dagger c_{2\uparrow}^\dagger c_{3\uparrow}^\dagger) 0\rangle$	$\frac{1}{\sqrt{2}}\left(\begin{array}{c} \uparrow\downarrow \\ \downarrow\uparrow \end{array}\right) - \left(\begin{array}{c} \downarrow\uparrow \\ \uparrow\uparrow \end{array}\right)$	U
$\frac{1}{\sqrt{2}}(c_{1\uparrow}^\dagger c_{2\downarrow}^\dagger c_{3\downarrow}^\dagger - c_{1\downarrow}^\dagger c_{2\uparrow}^\dagger c_{3\downarrow}^\dagger) 0\rangle$	$\frac{1}{\sqrt{2}}\left(\begin{array}{c} \uparrow\downarrow \\ \downarrow\downarrow \end{array}\right) - \left(\begin{array}{c} \downarrow\uparrow \\ \downarrow\downarrow \end{array}\right)$	
$\frac{1}{\sqrt{2}}(c_{1\uparrow}^\dagger c_{1\downarrow}^\dagger c_{3\uparrow}^\dagger + c_{2\uparrow}^\dagger c_{2\downarrow}^\dagger c_{3\uparrow}^\dagger) 0\rangle$	$\frac{1}{\sqrt{2}}\left(\begin{array}{c} \uparrow\downarrow \\ \uparrow\uparrow \end{array}\right) + \left(\begin{array}{c} \downarrow\uparrow \\ \uparrow\uparrow \end{array}\right)$	$U + 2J$
$\frac{1}{\sqrt{2}}(c_{1\uparrow}^\dagger c_{1\downarrow}^\dagger c_{3\downarrow}^\dagger + c_{2\downarrow}^\dagger c_{2\uparrow}^\dagger c_{3\downarrow}^\dagger) 0\rangle$	$\frac{1}{\sqrt{2}}\left(\begin{array}{c} \uparrow\downarrow \\ \downarrow\downarrow \end{array}\right) + \left(\begin{array}{c} \downarrow\uparrow \\ \downarrow\downarrow \end{array}\right)$	(3-fold)

B 18, 4945 (1978).

[22] K. I. Kugel and D. I. Khomskii, Sov. Phys. JETP 52, 501 (1981).

[23] F. Mila and F. C. Zhang, Eur. Phys. J. B 16, 7 (2000).

[24] We have examined the linear orbital operator term in Eq. (5). For the spin configurations considered in this paper, namely the C- or G-type antiferromagnets or ferromagnet, the contribution of this linear term to the energy vanishes.

[25] F. Mila, R. Shiina, F. C. Zhang, A. Joshi, M. Ma, V. Anisimov and T. M. Rice, Phys. Rev. Lett. 85, 1714 (2000).

[26] A. Joshi, M. Ma, and F. C. Zhang, Phys. Rev. Lett, 86, 5743 (2001).

[27] Y. Q. Li, D. N. Shi, M. Ma, and F. C. Zhang, Phys. Rev. Lett. 81, 3527 (1998).

[28] C. Ulrich, G. Khaliullin, J. Sirker, M. Reehuis, M. Ohl, S. Miyasaka, Y. Tokura, and B. Keimer, LANL preprint, cond-mat/0211589, (2002).